Detailed Mapping and Modeling of Urban Vegetation: What Are the Benefits for Microclimatic Simulations with Town Energy Balance (TEB) at Neighborhood Scale?

Émilie Bernard, Cécile De Munck, Aude Lemonsu

Detailed Mapping and Modeling of Urban Vegetation: What Are the Benefits for Microclimatic Simulations with Town Energy Balance (TEB) at Neighborhood Scale?

ÉMILIE BERNARD,[a,b] CÉCILE DE MUNCK,[a] AND AUDE LEMONSU[a]

[a] *CNRM, Météo-France/CNRS, Toulouse, France*
[b] *Université Gustave Eiffel, Bouguenais, France*

(Manuscript received 5 July 2021, in final form 13 April 2022)

ABSTRACT: Cities develop a specific climate related to their morphology and the materials that constitute them. The addition of vegetation in urban areas induces cooling and shading effects that can modify local climate and thermal comfort conditions. The Town Energy Balance (TEB) urban canopy model offers several configurations for a more or less fine-tuned consideration of natural covers and associated physical processes in the urban environment. This study aims to evaluate the sensitivity of TEB to the representation of vegetation and the resolution of the chosen databases in the simulation of microclimatic variables, at the scale of a heterogeneous urban neighborhood located in Toulouse, France. First, the effect of the improved description of the vegetation input to the model is highlighted by comparing the results obtained with a readily available national database and then with a very-high-resolution satellite-derived vegetation database. Second, the two vegetation parameterizations, with or without explicit tree stratum, that are available in the TEB model are evaluated and compared. Measurements carried out on specific routes and stop points in a neighborhood of Toulouse allowed microclimatic variables to be evaluated. Results show that refining the vegetation database can somehow improve the modeling of air temperature. As a result of enhancing the vegetation description in the model, that is, physical processes associated with the presence of trees in urban canyons, the air temperature, but also the wind and the thermal comfort index, are better simulated. These results are encouraging for the use of TEB as a decision support tool for urban planning purposes.

KEYWORDS: Databases; Model evaluation/performance; Urban meteorology; Vegetation–atmosphere interactions

1. Introduction

Urban areas are characterized by a complex morphology and are predominantly composed of artificial materials. This modifies the radiative, energetic, hydrological, and turbulent exchanges between the surface and the atmosphere in comparison with natural environments (Cleugh and Oke 1986; Mills 2008). Consequently, urban microclimate is different from the one of the surrounding countryside (Grimmond 2007) and leads in particular to the phenomenon of urban heat island (UHI; Oke 1988). Reintroducing vegetation and pervious surfaces in urban areas, however, can counterbalance this effect. It will have an inhibiting effect on UHI (Shashua-Bar et al. 2010) by reducing air temperature and therefore thermal comfort (Coutts et al. 2015; Armson et al. 2012). This effect is mainly due to the modification of exchange of energy through evaporation of soil water and the evapotranspiration of plants, the provision of shade and aerolic effects on the influence of airflow. The air is locally cooled (Qiu et al. 2013). The combined effect of low vegetation and trees found in urban parks is on average 0.94°C during the day, according to Bowler et al.'s (2010) meta-analysis. Depending on local conditions, this cooling tendency can be advected to adjoining streets (Upmanis et al. 1998) and influence surrounding areas. At the same time, some numerical studies have shown that the addition of watered vegetation in a city can significantly help cool the air in the streets (de Munck et al. 2018; Lee et al. 2016; Wang et al. 2018; Meili et al. 2021) and improve the thermal comfort of people (Joshi and Joshi 2015). All this suggests that the answer to the warming problem of cities lies partly in the greening of urban space. It is therefore of paramount importance to model the role of vegetation in urban canopy models (UCMs) as realistically as possible. This will help to better understand the present and future microclimate of cities and prevent the possible risks incurred by their inhabitants (high temperatures, thermal discomfort).

With the need of modeling tools for planning scenarios the majority of urban climate models take into consideration the effects of vegetation. It allows for a more realistic simulation of the energy balance (Grimmond et al. 2010, 2011) and microclimate (Shashua-Bar and Hoffman 2000; Shashua-Bar et al. 2010) at street level. In the scientific community, there are currently different levels of refinement to integrate vegetation in UCMs. The simplest level is to use a tile approach that treats natural and artificial covers separately using specific surface schemes (Lemonsu et al. 2004). In other models, vegetation can also be directly integrated in the urban canyon (Lemonsu et al. 2012; Lee and Park 2008; Lee and Baik 2011; Wang et al. 2012, 2021; Meili et al. 2020), which makes it possible to represent the radiative, energetic, and dynamic interactions between the artificial surfaces, the vegetation, and the air of the canyon. By defining more precisely vegetation characteristics, it then takes into account the evolution of water content in the subsurface layer and latent and sensible heat flux associated with vegetation. The most complex parameterizations consist in

Denotes content that is immediately available upon publication as open access.

Corresponding author: Émilie Bernard, emilie.bernard@meteo.fr

DOI: 10.1175/JAMC-D-21-0134.1

the representation of trees inside urban canyons. It was implemented by Lee and Park (2008), Lee and Baik (2011) for the first time. Their tree-lined urban canyon model explicitly represents tree crowns. Tree crown is characterized by the fraction of its surface that overlooks those on the ground, a thickness, and a leaf area density (LAD). However, this parameterization has been integrated in a single layer urban canopy model, contrary to the model Building Effect Parameterization with Trees (BEP-Tree) next developed by Krayenhoff et al. (2014, 2015, 2020) and Mussetti et al. (2020) that includes radiative effects such as shade, albedo, emissivity, storage of energy, and momentum drag of trees on wind flow in a multilayer canyon model. Ryu et al. (2015), meanwhile, chose to define streets trees in a single-layer model but add, to the last processes, hydrological effects with root water uptake. Recently the multilayer urban canopy model Town Energy Balance (TEB), historically developed by Masson (2000), has been refined, notably to model street trees (TEB-Tree, Redon et al. 2017, 2020). This new parameterization, inspired by Lee and Park's (2008) approach, allows for the modeling at the same time of radiative, dynamic effects, and evapotranspiration rates of trees inside urban canyons. It also offers the possibility to define different types of tree vegetation (deciduous, evergreen, etc.) characterized notably by their leaf area index (LAI), their albedo, and their emissivity.

The literature highlights the improvement of processes associated with vegetation in UCMs essential to carry out more accurate impact and adaptation studies in urban heterogeneous environments and their contribution to simulate microclimatic conditions. These improvements necessarily lead to a need for more precise data to describe the vegetation cover of cities, but the question of the availability or accuracy of such input data is rarely studied. Moreover, it is not always easy to provide, in reality, the spatial extent of the vegetation, the different strata and systems present (lawns, trees, building vegetated envelopes, etc.), their dimensions, and the species that make them up vary greatly from one city to another but also within each city. In practice, few databases already exist that provide this level of details. Administrative databases available so far generally only provide rough estimates of vegetated surfaces with rarely a distinction in strata, let alone species names/types. Whereas the simple tile approach could be satisfied with standard land-cover classifications such as Coordination of Information on the Environment (CORINE) Land Cover (Bossard et al. 2000; Buttner et al. 2004) on Europe or ECOCLIMAP (Faroux et al. 2013) on a global scale, more complex approaches, implying better mapping and characterization of vegetation, consequently require the development of precise vegetation databases (Masson et al. 2020). Remote sensing techniques combined with image processing, that allow large areas to be processed, are perfectly adapted to the collection of urban vegetation data.

In this context of diversity of parameterizations and databases for urban vegetation, it is important to understand the respective contributions of the more detailed parameterizations and databases to a better simulation of the urban microclimate. However, no study to date has attempted to answer this question using the contribution of such a high-resolution database and the latest tree vegetation parameterization included in the TEB model. To help provide some answers, we have chosen the scale of an urban neighborhood to evaluate and compare the performances of the urban canopy model TEB to simulate the microclimate locally, using two input databases of different precision and two levels of refinement to model urban vegetation (without or with consideration of tree strata). To do this, it was first necessary to build two databases describing the land cover of the study area, one with the precision usually available, the other more realistic with the details of the herbaceous and tree-lined strata. Then, by combining different databases and urban vegetation parameterizations, we evaluated the model's sensitivity to simulate the microclimate and the thermal comfort of the study area according to their respective levels of detail.

After a general overview of the model TEB and the specificities of its ground and high vegetation parameterizations in section 2, the vegetation databases produced for the sensitivity analysis are described in section 3. A presentation of the simulation configurations set up for the application of the model to a case study in Toulouse, France, follows in section 4. All results are presented and discussed in section 5. A first part is dedicated to the evaluation and comparison of vegetation databases. Then simulation results are presented and compared with observations, exploring air temperature at a neighborhood scale, then microclimatic parameters in different urban landscapes, and finally thermal comfort index. Conclusions and perspectives are given in section 6.

2. Modeling urban vegetation with TEB

Based on a parametric approach, the TEB model is able to model in a simplified way the fine-scale physical processes in the urban canopy, while sustaining the numerical ability to model urban climate at the scale of the entire city. It accounts for the interactions between urban surfaces and the surrounding air. This multilayer canopy model represents the different elements (road, building walls and roofs) of an average street canyon considered to be of infinite length.

a. Physical processes

To take into account the interactions between the vegetation in cities and the built environment, Lemonsu et al. (2012) integrated urban ground-based vegetation in the street canyon. This TEB-Veg parameterization allows for street canyon widths closer to reality, while imposing more realistic meteorological forcings to vegetation, that is, the shadow effects from walls, the impact of built surfaces on street-canyon wind speed, air temperature and humidity. Based on the Interactions between Soil, Biosphere, and Atmosphere (ISBA) model (Boone et al. 1999; Decharme et al. 2011), TEB-Veg has the ability to differentiate different types of urban vegetation via different biophysical characteristics (LAI, stomatal resistance, albedo, emissivity, etc.). Although the ISBA model differentiates between bare soil, herbaceous vegetation, and tree vegetation in terms of input data, the descriptive and physiological parameters associated with each type are then averaged over each grid

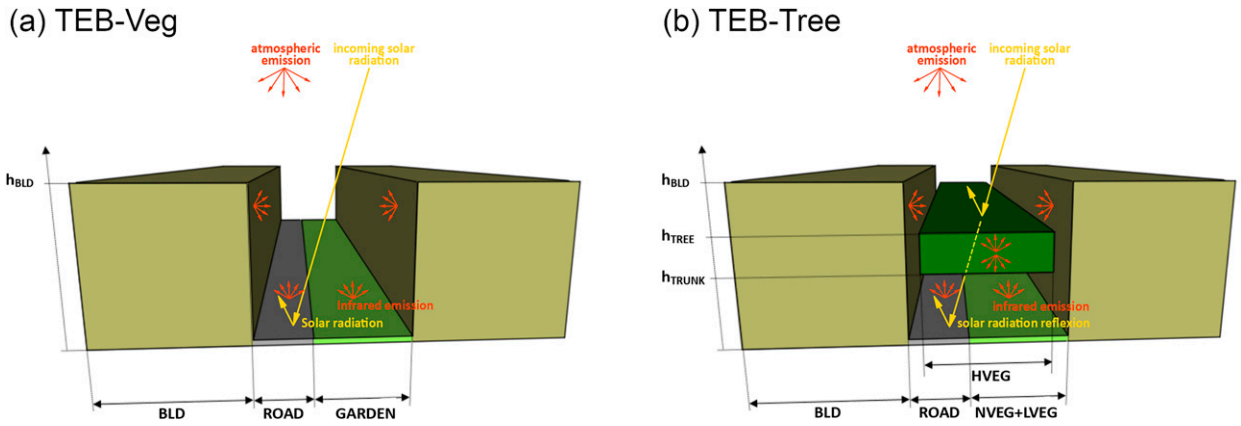

FIG. 1. Description of canyon configuration and main radiative processes with (a) TEB-Veg and (b) TEB-Tree parameterizations: incoming solar radiation and infrared radiation are represented by the solid yellow lines and the red lines, respectively.

cell of the modeling domain to describe a composite soil-plant compartment. This approach is called bigleaf. In TEB-Veg, this compartment is considered inside the canyon at ground level without vertical extent.

To improve the description of vegetation strata, Redon et al. (2017, 2020) subsequently added, with the TEB-Tree parameterization, a separate layer for tree foliage: the foliage strata, which overlaps the ground fractions occupied by low vegetation or asphalt, is characterized by a coverage fraction, a mean height, and a vertical extent.

1) RADIATIVE BALANCE

TEB-Veg already accounts for the obstruction effect of buildings on incident radiation for natural covers and the multiple radiative reflections inside the canyon between walls, road, and ground-based natural covers. The tree layer implemented in TEB-Tree now impacts the interception, absorption, and transmission of the incoming solar and infrared radiation at the top of the urban canopy layer (Fig. 1). It comes into play in the complex radiative interactions between all the elements of the canyon. Especially, trees can shade facades, roads, and gardens, and are an additional source of infrared emission.

2) TURBULENT EXCHANGES

The evolution of microclimatic variables (temperature, humidity, and wind) is modeled according to several vertical levels that make discrete the air layer from the ground to the top of the urban canopy layer using the TEB-Surface Boundary Layer (SBL) parameterization (Hamdi and Masson 2008; Masson and Seity 2009). From Yamada (1982), it accounts for the contributions of the ground-based surfaces, the walls, and the roof for the computation of sensible and latent heat fluxes and drag effects. TEB-Veg takes into account the drag force due to buildings only (Lemonsu et al. 2012), whereas TEB-Tree now adds the drag force of the trees through a drag coefficient depending on leaf density profile, which impacts the airflow in the street canyon (Redon et al. 2020). While TEB-Veg assumes that turbulent fluxes from the natural canopy compartment come from the ground, TEB-Tree includes a vertical redistribution of the turbulent fluxes between ground-based natural covers and tree-foliage layer to better simulate their potential impacts on the vertical profile of microclimatic variables.

3) UNIVERSAL THERMAL CLIMATE INDEX

TEB computes the universal thermal climate index (UTCI) for the outdoor environment, which is a human-body comfort index defined by Bröde et al. (2012). UTCI depends on air temperature, humidity, wind speed conditions, and mean radiant temperature (Kwok et al. 2019) within the canyon. The latter is calculated from the ensemble of the radiation sources received by the person, including incoming shortwave radiation (direct and diffuse), radiation reflected on the walls and the ground, longwave radiation from the atmosphere, and infrared emissions from all the canyon surfaces. In TEB-Tree, the calculation of UTCI is adapted so as to consider the impact of the tree foliage layer on mean radiant temperature (Redon et al. 2020).

For more details on the physical processes and evaluation described in TEB-Veg see Lemonsu et al. (2012), for radiative effects of trees of TEB-Tree see Redon et al. (2017) and for energetic and dynamic effects Redon et al. (2020).

b. TEB input parameters related to natural covers

In addition to the standard urban parameters required by TEB including land-use fractions, geometric parameters, and radiative and thermal properties for buildings and road, specific parameters are required for modeling soil and vegetation.

For TEB-Veg version that describes natural covers by a composite compartment on the ground, the land-cover fractions are defined without overlapping of strata. The ground-based surface of the canyon consists of a combination of road, bare soil, and low and high vegetation. For an urban grid cell, the sum of cover fractions of these elements added to the fraction of buildings equals 100%. The prescribed input data also define the albedo and emissivity of each nature element independently, as well as leaf area index, stomatal resistance, and

TABLE 1. Main descriptive parameters of the urban canyon in the TEB model, including specific data for natural covers. Parameters are prescribed by users except for those indicated with an asterisk, which are generally derived from vegetation types and empirical relationships.

Parameters	Symbol	Unit
Land-cover fractions		
Cover fraction of buildings	BLD	—
Cover fraction of ground-based impervious covers	ROAD	—
Cover fraction of ground-based natural covers	GARDEN	—
Cover fraction of bare soil	NVEG	—
Cover fraction of low vegetation	LVEG	—
Cover fraction of high vegetation	HVEG	—
Canyon geometric parameters		
Mean building height	h_{BLD}	m
Wall plan area ratio	r_W	—
Canyon aspect ratio	$h_{BLD}/W = 0.5r_W/(1 - BLD)$	—
Specific data for natural covers		
Type of low and high (tree) vegetation	$VTYP_{LVEG}$; $VTYP_{HVEG}$	—
Height of trees	h_{TREE}	m
Height of trunks	h_{TRUNK}	m
Albedo of soil, low, and high vegetation*	α_{NVEG}; α_{LVEG}; α_{HVEG}	—
Emissivity of soil, low, and high vegetation*	ε_{NVEG}; ε_{LVEG}; ε_{HVEG}	—
LAI of low and high vegetation	LAI_{LVEG}; LAI_{HVEG}	$m^2\ m^{-2}$
LAD of high vegetation*	LAD_{HVEG}	$m^2\ m^{-3}$
Min stomatal resistance of low and high vegetation*	$RSmin_{LVEG}$; $RSmin_{HVEG}$	$s\ m^{-1}$
Root fraction profile of low and high vegetation*	$Froot_{LVEG}$; $Froot_{HVEG}$	—

root profile separately for low and high vegetation, and tree height. These parameters are then aggregated for the composite compartment.

For TEB-Tree, since trees are no longer on the ground but constitute a supplementary stratum, the cover fractions are expressed differently. The canyon ground consists of road, bare soil, and low vegetation. The cumulative fraction of these covers added to building fraction is 100%, whereas the tree cover fraction is independent. The parameters are aggregated only for the ground-based compartment composed of the bare soil and low vegetation. Trees are defined by their own parameters including their total height and height of trunks, which allows TEB to compute the vertical extent and LAI profile of tree crowns. The physical characteristics and ecophysiological properties of trees considered are featured in Table 1 with descriptive parameters of the urban canyon.

3. Creation of a suitable database for modeling natural areas in cities

This section presents the methodology developed to provide a database sufficiently precise for TEB. The challenge is to establish a methodology that can be replicated and applied to most cities owning an urban database, even if it is different from the one used in this study.

a. Land-use mapping with BD TOPO data

One of the mission of the French National Institute of Geographical and Forest Information (IGN) is to draw up a cartographic inventory of the landscape elements that make up the French territory. We chose to work from their BD TOPO map database, which has the advantages of being available for all French cities, relatively exhaustive, regularly updated, and free to access for research applications. It provides sufficient information to derive a cartography of urban parameters that are requested for urban modeling purposes: the urban artificial surfaces such as buildings (with their heights) and roads as well as vegetation and water surfaces. A processing of this database is necessary to meet the model needs. Details of this processing are available in appendix A.

A postprocessing is required to map urban areas (including vegetation) and derive input parameters for TEB in the right format. First, a width is assigned to road and railway linear data in order to convert them into surface, and then to ensure the consistency with vectorial layers. The different surface layers are then merged into a single land-cover layer without any overlapping, by prioritizing them according to the level of confidence in each layer: 1) buildings (greater reliability), 2) water surfaces (mostly under other typologies encountered, e.g., under a bridge), 3) vegetation (vector layer, considered more trustworthy than linear associated with a buffer), 4) bare soil (i.e., railways and unpaved paths, most uncertain data), and 5) asphalt (estimated from the width associated with each road linear). The remaining undefined areas are associated with ground-based asphalt surfaces (i.e., car parks and roads) based on verification with aerial photograph. The final result is a 1-m-spatial-resolution land-use map called thereafter "TOPO." These treatments have been deliberately designed to have a simple and reproducible method for land-use classification with a free GIS software (QGIS, version 2.14).

b. Contribution of very-high-resolution vegetation data

The BD TOPO database is of very high quality to map buildings, paved surfaces, and water. Nevertheless, it reveals a lack of accuracy with respect to urban vegetation. It tends to underestimate its coverage, especially in residential areas where vegetation of private spaces is often not mapped (Crombette 2016). Therefore, an alternative method is investigated to produce a more accurate mapping of urban vegetation, both in terms of spatial coverage and distinction of the different strata. A very-high-resolution vegetation database with a 0.5 m spatial resolution is used. The one is derived from Pléiades optical satellite images by Crombette et al. (2014) at very high resolution in multispectral mode (2.7 m) and in panchromatic mode (0.7 m) taken in May 2012 resampled at 0.5 m (https://earth.esa.int/web/eoportal/satellite-missions/p/pleiades). Low vegetation (grass) and high vegetation (shrubs and trees) were distinguished by applying a threshold on the NDVI map, initially produced from infrared and near-infrared Pléiades images. These two new layers of vegetation are substitute to the previous BD TOPO vegetation layer before applying the same method as previously for prioritizing and merging surfaces layers (section 3a). This second land-use map is called PLEI herein.

c. From land-cover databases to input parameters for the model

From the two 0.5-m-spatial-resolution land-cover classifications that were derived, two sets of input parameters for the Surface Externalisée (SURFEX) land modeling system (Masson et al. 2013) are computed according to a modeling grid chosen at the resolution of 100 m. In SURFEX, each land-cover type is treated by different models, such as TEB for urban covers and ISBA for natural covers (including urban vegetation; see section 2).

1) LAND COVER

First, the respective fractions of land covers within each 100 m × 100 m grid mesh of the study area (Fig. 2) are computed according to the number of pixels occupied by each type of land cover considered (buildings, asphalt, bare soil, low vegetation, high vegetation, and water). However, at this stage, there is yet no distinction between the natural and the urban vegetation.

2) DISTINCTION BETWEEN URBAN AND NATURAL VEGETATION

Second, a statistical test was conceived and run to distinguish the urban vegetation (that is part of and influenced by the urban landscape) from the natural vegetation. Both types of vegetation will later be treated by specific surface schemes: urban vegetation by TEB, whereas natural vegetation by the ISBA model. The vegetation of grid meshes was classified into three categories according to the ratio of the building cover fraction to the unbuilt cover fraction (i.e., bare soil, low and high vegetation, and water surfaces) of the mesh and user-defined thresholds (Fig. 3): (i) the vegetation is totally natural when there is no building in the grid cell, that is, ratio = 0%; (ii) vegetation is considered part of the urban environment when the buildings cover more than 2% of the grid cell, that is, ratio > 2%; (iii) for the intermediate case, the vegetation is separated into a proportion of urban vegetation defined as twice the fraction of buildings in the mesh, that is, ratio ≤ 2%, the remaining fraction being prescribed as natural vegetation without interaction with built-up covers. The TOWN fraction for each grid cell then corresponds to the fraction of impervious surfaces and urban vegetation.

3) TREE VEGETATION MORPHOLOGICAL PARAMETERS

The tree characteristics are not available at the resolution of the vegetation strata. Based on expert knowledge of the neighborhood studied tree heights are simply prescribed to 10 m or as high as the mean height of the buildings of the mesh if buildings are less than 10 m high. Trunk's heights are prescribed to be one-third of tree heights. Tree crowns are assumed to have the shape of a cylinder and a vertical extension of two-thirds of the tree.

4. Evaluation framework for model sensitivity

a. Experimental data

Within the context of the Evaluation Multidisciplinaire et Requalification Environnementale des Quartiers (EUREQUA) research project (Haouès-Jouve et al. 2022), an experimental campaign took place in the neighborhood Tabar-Papus-la Fourguette-Bordelongue (Fig. 2) in the southeast of Toulouse. It is distinguished by a varied urban fabric: detached private houses with gardens (HWG), 5-story buildings and two high-rise buildings of 14 stories with little vegetation (LBD), as well as high-rise buildings (HBD) of different heights surrounded by green spaces with trees. This landscape heterogeneity is likely to induce microclimatic variations between these different types of urban fabrics. This is one reason why it was chosen as a case study. During the experiment, mobile measurements at 2 m of microclimatic parameters were collected by walking along a predefined route (Haouès-Jouve et al. 2022). More specifically, an intensive observation period (IOP) of three consecutive days took place from 17 to 19 June 2014 with instrumented routes every 3 h. The data recorded consist of air temperature, relative humidity, wind speed, and gray-globe temperature [see the description of the mobile system in Lemonsu et al. (2019)] in order to calculate mean radiant temperature and UTCI. Nine stop points provided longer measurements of microclimatic variables. Their locations and characteristics are shown in Fig. 4.

For each instrumented route, a spatial adaptation was applied in order to project and aggregate all the records on the same averaged and idealized route composed of georeferenced and equidistant points of 20 m, which allows a direct comparison of all routes together. A time correction was also made in order to remove the synoptic-scale temporal evolution of temperature along each route and recalibrate the records in accordance with the departure time of each route (Le Bras 2015).

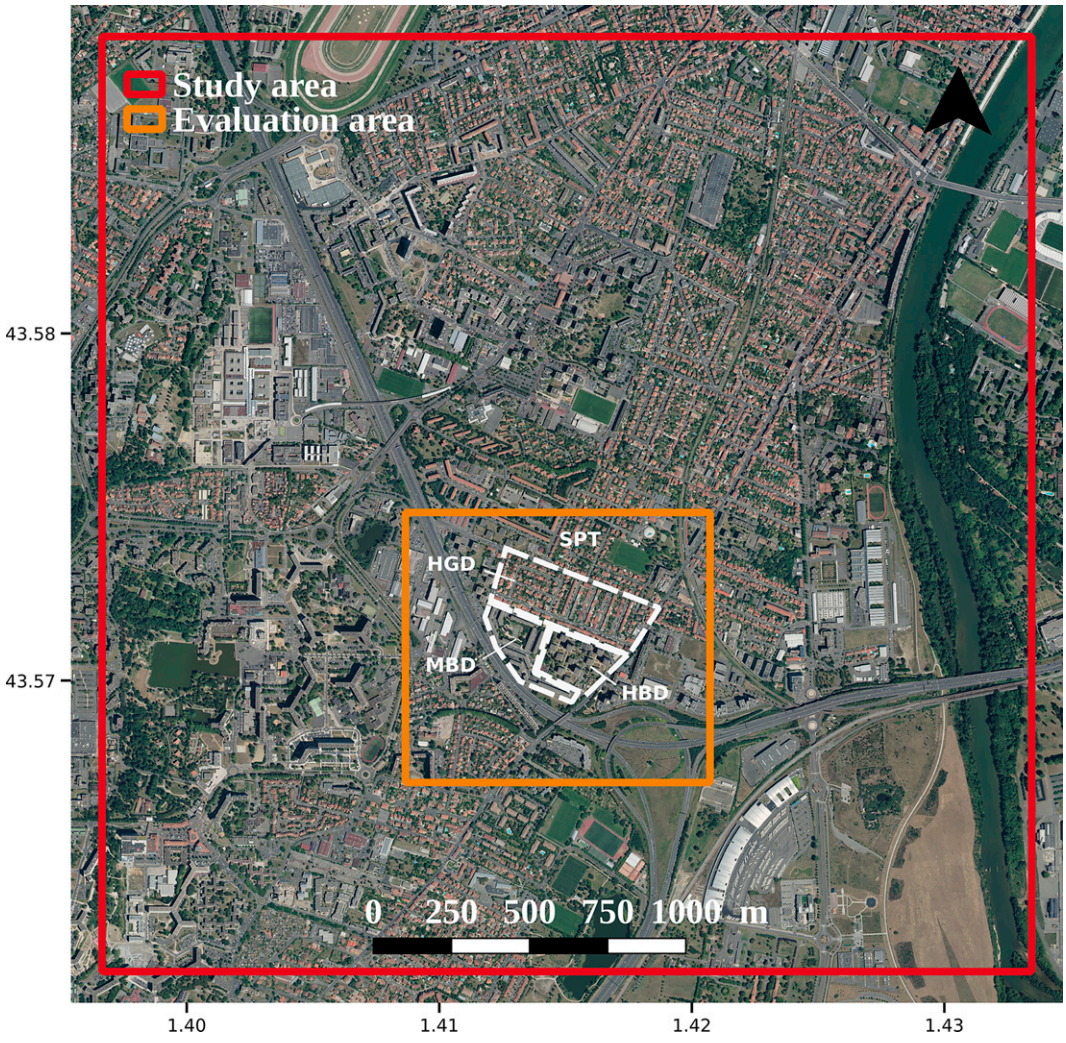

FIG. 2. Map representing the limits of the neighborhood studied in Toulouse: the red-outlined square represents the modeled study area, the orange-outlined one indicates the evaluation area for the land-cover databases computed. The white dotted line distinguishes the homogeneous neighborhoods of the evaluation area, as defined in sections 4a and 5b(3).

b. *Common base for all simulation configurations*

The three days of the IOP are simulated with the MesoNH nonhydrostatic atmospheric model (Lafore et al. 1998) coupled to the SURFEX land surface modeling system including TEB. To go down to the horizontal resolution of 100 m on the neighborhood studied, a configuration involving three nested grids is used in two-way mode (Fig. 5): Grid 1 runs over an area of 216 km × 216 km in the southeast of France with a spatial resolution of 600 m (domain 1). This domain is initialized and forced at its lateral boundaries by large-scale meteorological conditions provided by the reanalyses of the weather forecast model AROME (Météo-France). Grid 2 zooms on the agglomeration of Toulouse at a resolution of 200 m covering 32 km × 32 km (domain 2). Grid 3 finally runs on the studied area (domain 3; 3 km × 3 km) at the spatial resolution of 100 m. Appendix C contains the spatial definition of the surface parameters.

c. *Specific simulation configurations for urban vegetation*

For the grid with the highest horizontal resolution (domain 3), three specific configurations (summarized in Table 2) were set up to evaluate the impact of more or less realistic description of urban vegetation with regard to input data precision and level of refinement of the parameterizations. The reference configuration (Veg-TOPO) relies on the standard configuration usually applied to model urban spaces with vegetation, that is, the TEB-Veg parameterization (Lemonsu et al. 2012) and the TOPO database to define input parameters. The second configuration (Veg-PLEI) still uses the TEB-Veg parameterization but with the PLEI database and the third one (Veg-TREE) uses the new version of TEB (Redon et al. 2017, 2020) combined with PLEI. Therefore, the comparison of Veg-TOPO with Veg-PLEI first makes it possible to evaluate the benefit of more precise vegetation

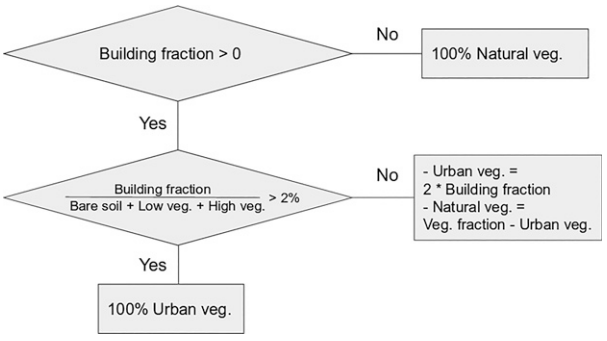

FIG. 3. Flowchart describing the conditions under which vegetation is classified as urban (in TOWN fraction) or natural (in NATURE fraction) vegetation.

description to prescribe model input data. The comparison of Veg-PLEI with Veg-TREE then makes it possible to investigate the gain potential brought by a refined parameterization of vegetation strata with regard to physical processes.

5. Results and discussion

a. Evaluation of developed databases on a case study

The methodology developed in section 3 is applied to characterize the land use of the study area.

As part of the French National Research Agency project EUREQUA (Haouès-Jouve et al. 2022), a land-use map was produced for this neighborhood, but on a smaller area (Fig. 2). This cartography was based on the BD TOPO of the IGN and on a manual digitization of the bare soil and vegetation zones distinguishing the herbaceous, shrub and tree layers (referred to herein as REAL). It is considered here as the ground truth for the evaluation of the two maps TOPO and PLEI produced for the studied neighborhood, on the area they have in common (Fig. 6). The respective land-cover percentages of each type of surface over the evaluation area are compared in Table 3. Note that for comparing the three maps together, the different vegetation layers available in REAL and PLEI are merged into a single layer to match TOPO categories. The cover fractions of buildings and water

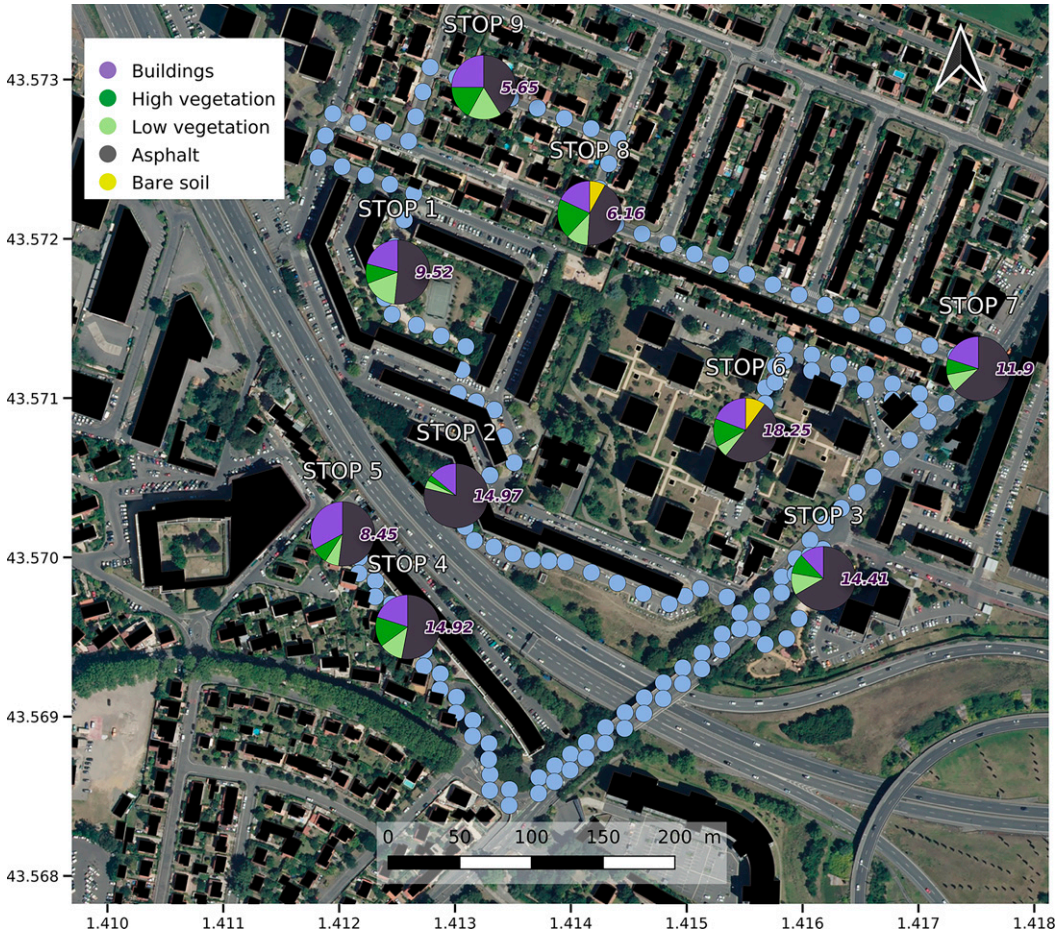

FIG. 4. Photograph of the studied neighborhood (evaluation area; Fig. 2) in Toulouse with routes and nine stop points: pale blue points indicate the route chosen for the instrumented mobile measurements. For each stop point, pie charts show the land-cover fraction of buildings in purple, high vegetation in dark green, low vegetation in light green, bare soil in yellow, and asphalt in gray. The number on the pie charts is the mean building height of buildings of the grid mesh.

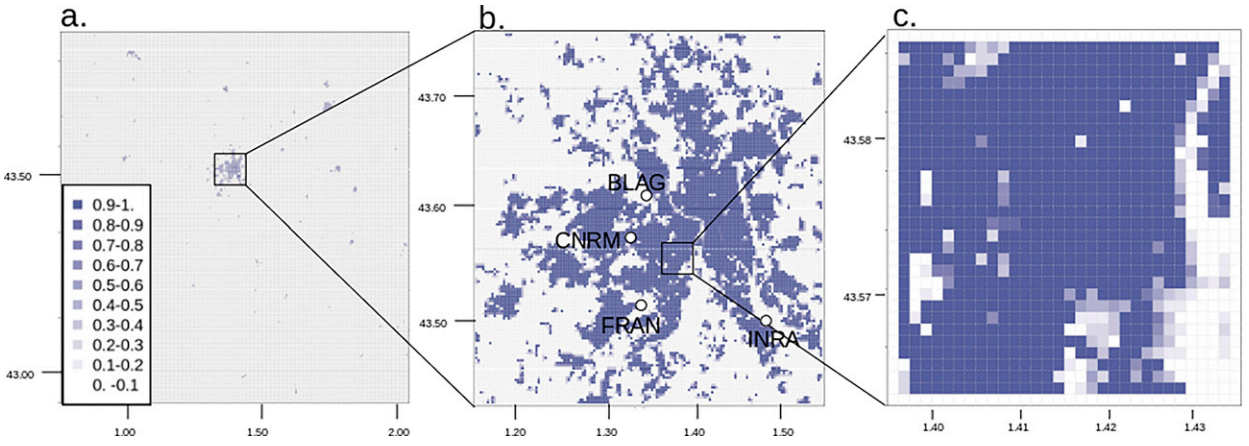

FIG. 5. Simulation nesting, as given by maps of the three nested domains of simulation represented by their town fraction (impervious surfaces and urban vegetation): the (a) southeast of France, (b) city of Toulouse, and (c) neighborhood studied (study area; see Fig. 4).

of TOPO and PLEI are very close to those of REAL since they are all derived from the same BD TOPO source. PLEI allows for a better description of the total vegetation coverage of the area than TOPO, with respective percentages of 35.1% and 11.2% as compared with 39.3% in REAL. Bare soil areas are largely underestimated by both TOPO and PLEI by up to 7.0% because they are not initially mapped in BD TOPO, like in most databases around the world. In this methodology, only unpaved paths are included in the bare soil layer. By method design, the undersampling of vegetated and urban soil areas results in an underestimation of asphalt ground-based surfaces since any undefined areas is equated to this cover type: they represent a total fraction of 71.5% for TOPO, 47.6% for PLEI, as compared with 34.8% for REAL.

In addition, TOPO and PLEI are compared pixel by pixel with REAL through a confusion matrix (Table 3), which counts, for each database produced and each class, the number of misclassified pixels and the classes to which they are mistakenly assigned.

The classification quality of each database is evaluated using the kappa coefficient, that is, the ratio between the error associated with the classification performed and the error associated with a random classification. According to the kappa thresholds established by Landis and Koch (1977), PLEI shows a good consistency with REAL (kappa = 0.64), with a significant improvement relative to TOPO (kappa = 0.36) due to a better mapping of vegetation. However, a bias persists because bare soil areas are significantly underestimated and misclassified in majority as asphalt. The overall accuracy translates the proportion of ground truth that is mapped correctly. Not surprisingly, TOPO shows a reasonable overall accuracy of about 56% while PLEI reaches 75%. If class-by-class results are analyzed, buildings are well mapped since they are based on data from the BD TOPO of the IGN whatever the method with an accuracy of 87.6% and 87.4% for TOPO and PLEI, respectively. The most significant difference between TOPO and PLEI lies in the vegetation class since the data sources are not the same. The accuracy is only 22.4% for TOPO, which greatly underestimates vegetation cover and consequently overestimates impervious ground surfaces. The accuracy is much better for PLEI (73.9%) even if an underestimation persists. In conclusion, PLEI, makes it possible to significantly improve the mapping of vegetation (both strata combined) relative to the initial TOPO database. Moreover, it presents the advantage of being able to be produced automatically on any study area on which this type of satellite images is available.

To evaluate the performance of PLEI to distinguish low and high vegetation strata, a second pixel-by-pixel comparison with REAL is undertaken by keeping all land-cover classes (Table 4). The agreement of PLEI with ground-truth is moderate with a kappa coefficient of 0.51 and an overall accuracy of 63%. This results come from an overestimation of high vegetation coverage by the NDVI-based method applied to Pléiades imagery, which tends to classify shrub vegetation as high vegetation (Crombette 2016). Consequently, the user's accuracy for low vegetation is only of 17.4%. The accuracy for high vegetation remains good with 71.5%. In addition, the foliage of trees seen from satellite imagery may mask road surfaces, which can explain why road is better represented by TOPO according to the user's accuracy (Table 3).

TABLE 2. Specific simulation configurations for urban vegetation and the domain-3 model at 100-m resolution.

Configurations	Parameterization	Database	Characteristics
Veg-TOPO	TEB-Veg	TOPO	Reference simulation
Veg-PLEI	TEB-Veg	PLEI	Improved vegetation database relative to reference
Tree-PLEI	TEB-Tree	PLEI	Improved vegetation database and modeling of vegetation strata

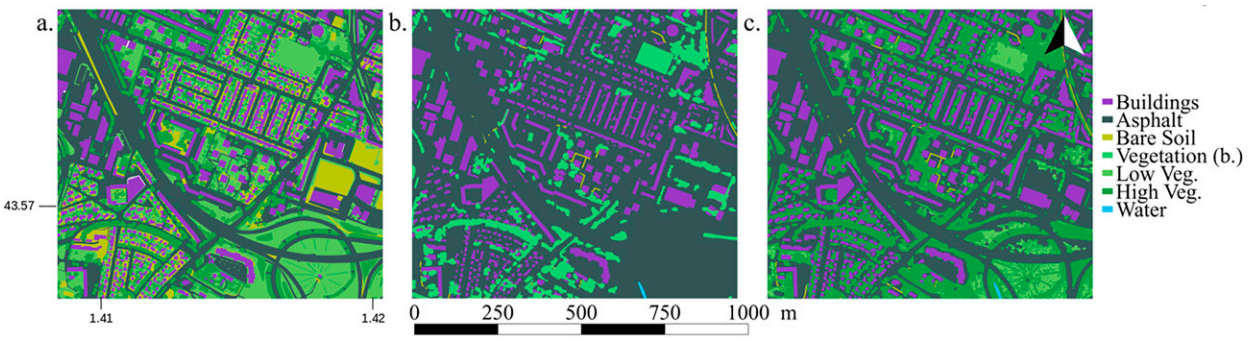

FIG. 6. Land-cover maps of the evaluation area (Fig. 2): (a) REAL, (b) TOPO, and (c) PLEI.

b. Evaluation of simulated microclimate variables

The data of instrumented routes make it possible to characterize the very-fine-scale variations in microclimatic variables at street level. The sensitivity of model performances was first investigated for the study area by the comparison of the air temperature observed along the instrumented routes and simulated (within domain 3 of Fig. 5), and then at specific stopping points of the routes that are representative of different urban landscapes that are more or less vegetated. Before that, the evaluation of the simulated synoptic conditions showed a good agreement with the meteorological variables recorded by surface stations (within domain 2 of Fig. 5; for more details, see appendix B).

1) TEMPERATURE VARIABILITY ALONG THE ROUTES

Two levels of model performance analysis are proposed here: 1) the results of the experiments are first compared with the observations in terms of temperature standard deviation for each instrumented route in order to evaluate the abilities of the model to reproduce a realistic level of spatial variability of temperature across the study area; 2) the experiments are then compared on the basis of the RMSE and MBE calculated for each instrumented route in order to evaluate the overall performance of the model in simulating air temperatures along the route.

The temperature records along the 19 instrumented routes are presented in Fig. 7a including 7 night routes made between 2100 and 0600 local time and 12 day routes made between 0900 and 1800 local time. Two main regimes stand out for nighttime (bottom subset) and daytime (top subset) measurement periods. The temperature variability during a same route is clearly higher during the day than during the night (respectively on average 3.2° and 1.9°C).

Figure 7b presents the standard deviation (SD) of observed and simulated air temperatures for each route. Variability of observations for each routes, associated with SD, is well represented by the model but is higher (median of 0.5°C) than the one simulated with the three configurations (median between 0.2° and 0.3°C). Tree-PLEI simulates more spatial

TABLE 3. Confusion matrix for TOPO and PLEI compared with REAL (ground truth), indicating the number of pixels associated with each class. The respective percentages of land use are indicated in italics next to each typology. For TOPO vs REAL, the overall accuracy = 56.65% and the kappa coefficient = 0.36. For PLEI vs REAL, the overall accuracy = 75.49% and the kappa coefficient = 0.64.

		REAL					
	Proportions	Buildings *17.75%*	Asphalt *34.85%*	Water *0.06%*	Bare soil *8.01%*	Vegetation *39.33%*	Producer accuracy
TOPO							
Buildings	*16.50%*	524 420	9300	0	8996	14 001	94.20%
Asphalt	*71.50%*	70 833	1 088 404	1824	244 336	1 006 662	45.10%
Water	*0.05%*	0	0	0	0.00	1679	0.00%
Bare soil	*0.75%*	35	17 529	0	567	6823	2.30%
Vegetation	*11.20%*	3604	60 381	146	16 105	297 855	78.80%
User accuracy		87.60%	92.60%	0.00%	0.20%	22.40%	
PLEI							
Buildings	*16.50%*	523 647	9594	0	9086	14 384	94.10%
Asphalt	*47.92%*	57 614	1 041 752	1439	188 307	327 405	64.4%
Water	*0.05%*	0	0	0	0	1807	0.00%
Bare soil	*0.43%*	31	11 352	0	306	2565	2.10%
Vegetation	*35.10%*	17 600	112 916	531	72 305	980 859	82.80%
User accuracy		87.40%	88.60%	0.00%	0.10%	73.90%	

TABLE 4. Confusion matrix for PLEI compared with REAL (ground truth), indicating the number of pixels associated with each class, including two vegetation strata. The respective percentages of land use are indicated in italics next to each typology. The overall accuracy = 63.17%, and the kappa coefficient = 0.51.

		REAL						
	Proportions	Buildings *17.75%*	Asphalt *34.85%*	Water *0.06%*	Bare soil *8.01%*	High vegetation *18.35%*	Low vegetation *20.98%*	Producer accuracy
PLEI								
Buildings	*16.50%*	523 647	9594	0	9086	4006	10 378	94.10%
Asphalt	*47.92%*	57 614	1 041 752	1439	188 307	157 895	169 510	64.40%
Water	*0.05%*	0	0	0	0	1762	45	0.00%
Bare soil	*0.43%*	31	11 352	0	306	1634	931	2.10%
High vegetation	*30.72%*	17 488	109 985	531	61 772	442 623	403 981	42.70%
Low vegetation	*4.38%*	112	2931	0	10 533	11 468	122 787	83.10%
User accuracy		87.40%	88.60%	0.00%	0.10%	71.50%	17.40%	

variability than the other two configurations, leading to standard deviations in better agreement with those observed.

In addition, Figs. 7c and 7d represent respectively the mean bias error (MBE) and the root-mean-square error (RMSE) of the temperatures of the routes simulated with the three configurations. These statistical scores confirm the best performance of Tree-PLEI, which displays the lowest errors (1.05°C median MBE and 0.3°C for median RMSE). The underestimation of the mean temperature by Tree-PLEI suggests that the model does not capture well enough on this scale the sudden and significant warming of the air due to incoming radiation at this time of the day, because it is a very localized phenomenon. When compared, Veg-TOPO shows a larger overestimation than the two other simulations, with higher

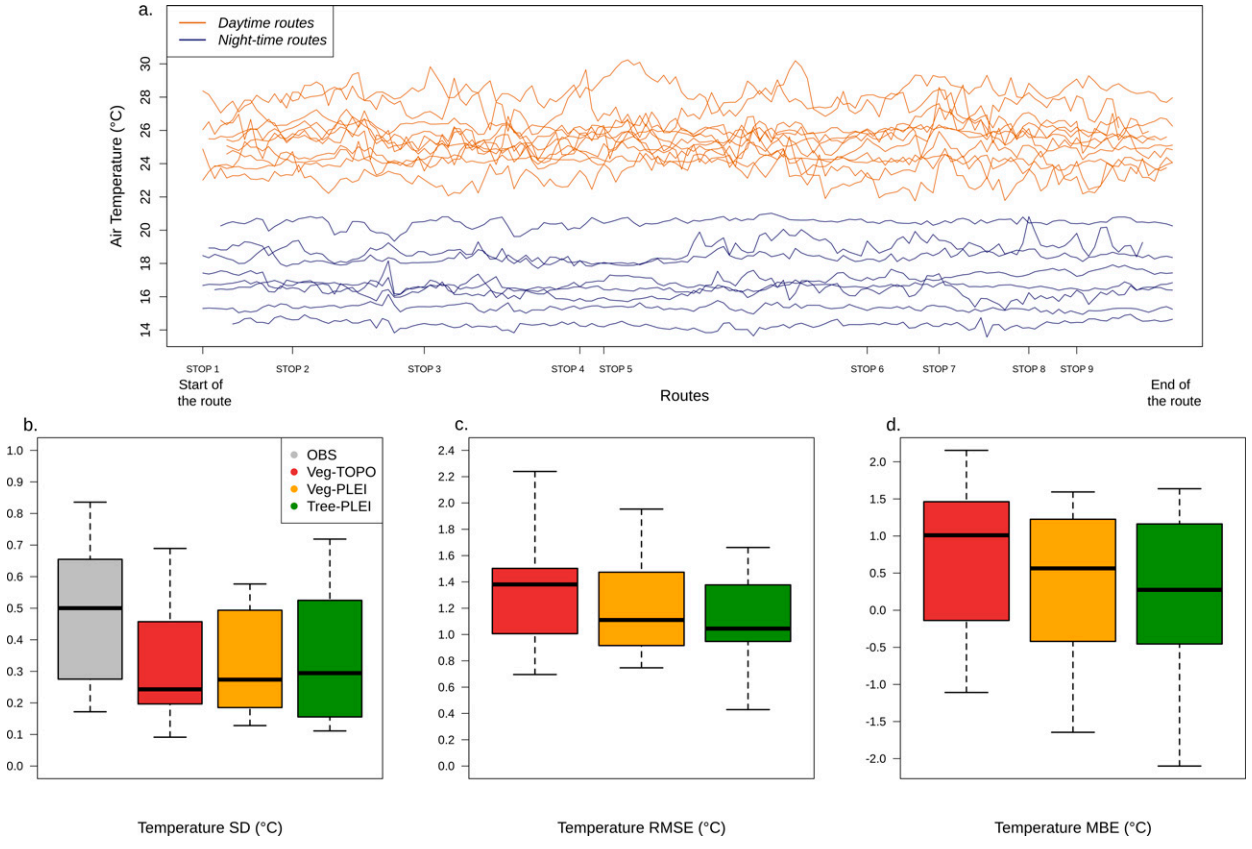

FIG. 7. Evaluation of the representativeness of the 2-m mean air temperature simulated during the 19 instrumented routes: (a) evolution of the temperature observed over time for each route, (b) boxplot of air temperature standard deviation for observations and each simulation configuration, (c) boxplot of temperature RMSE for each route and each simulation configuration, and (d) boxplot of temperature MBE for each route and each simulation configuration.

TABLE 5. Surface parameters associated with model grid meshes of STOP 6 and STOP 9. The ground fractions sum to 100%, with high vegetation overlapping the ground.

	STOP 6		STOP 9	
	TOPO	PLEI	TOPO	PLEI
Low vegetation fraction (%)	7	11	2	34
Bare soil fraction (%)	2	19	0	0
Building fraction (%)	19	19	25	25
Asphalt fraction (%)	72	51	73	41
High vegetation (%)	6	26	6	34
Building height (m)	18.25	18.25	5.65	5.65
Canyon aspect ratio (—)	0.50	0.50	0.35	0.35
Height of trees (m)	—	10.0	—	5.6
Height of trunks (m)	—	3.3	—	1.9

RMSEs ranging from 0.7° to 2.3°C and higher MBEs between −1.1° and 2.3°C. Veg-PLEI is more homogeneous and shows better scores than Veg-TOPO, with median MBE of 0.5°C and RMSE of 1.1°C, but does not achieve the best simulation score. This illustrates the good overall performances of the model.

2) COMPARISON OF MICROCLIMATE FOR TWO DIFFERENT URBAN LANDSCAPES

Nine stops of about 2 min (referred to as STOP 1–9) were made along instrumented routes (see locations in Fig. 4) to obtain more stable and therefore more reliable measurements, especially for wind and comfort indices. Here, STOP 6 and STOP 9 are chosen for a detailed analysis because they both have interesting particularities related to urban landscape (Fig. 4; Table 5). For the seven other stop points evaluated, scores are compiled in appendix D. They are both surrounded by a significant coverage of vegetation, composed of both low vegetation and trees, which allows for the contribution of databases and more precise parameterizations to be appreciated. They are nonetheless located in built environments with different morphologies, which makes it possible to study the impact of urban vegetation in contrasting urban environments. STOP 6 is surrounded by high-rise buildings, resulting in building heights and density larger than around the other stops (average height of 18.25 m). STOP 9 is located in the heart of a residential area composed of detached houses with lower buildings (average height of 5.65 m) and private gardens.

With TOPO, both STOP 6 and STOP 9 have very little vegetation, either low or high vegetation, and their fractions of sealed surfaces are close (Table 5). With PLEI, high and low vegetation are more important, thus reducing the road fractions (Fig. 8). STOP 6 is constituted with more bare soil than STOP 9. The differences in high vegetation (HVEG) fraction are significant, hence these two stops seem suitable to compare the impact of taking into account the vegetation (description and modeling) on the simulation results. The microclimatic parameters evaluated are air temperature, wind speed, specific humidity and UTCI. The comparison of time series is

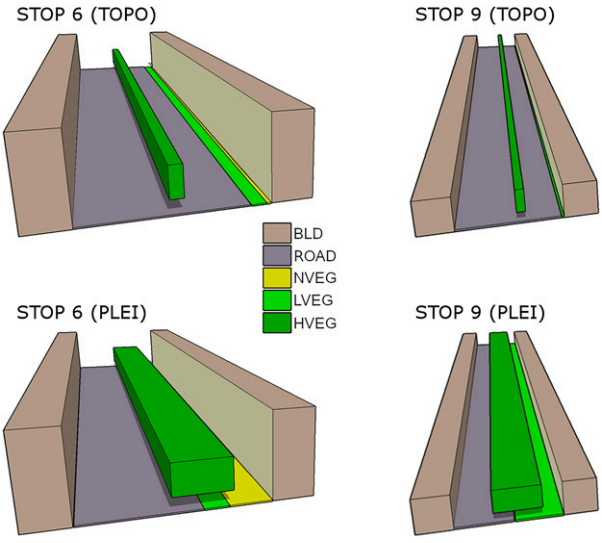

FIG. 8. Schematic representation of cover-type fractions and canyon morphology applied in TEB for both (top) Veg-TOPO and (bottom) Veg-PLEI configurations for the two studied locations at (left) STOP 6 and (right) STOP 9.

presented in Fig. 9 and completed by the statistical scores in Table 6. Figures 9a and 9b show that the air temperature is systematically overestimated by Veg-TOPO with an MBE around 0.50°C and a RMSE of 1.32°C on average for both stops and maximum biases at midday exceeding 2°C. This defect is the result of a strong overestimation of the cover fractions of impervious ground-based surfaces in the input database (see Table 5). They warm and store heat more efficiently than natural covers, and warm ambient air by turbulent exchanges. Veg-PLEI reduces the diurnal temperatures through a better characterization of natural (and therefore asphalt) covers. Simulated temperatures are consequently in better agreement with observations although, especially for maximum temperatures. The parameterization of street trees used in Tree-PLEI is close to Veg-PLEI but still provides the best results for both stop points (Table 6) with MBE less than ±0.19°C for STOP 6 and RMSE not exceeding 1.23°C for STOP 9. The improvement is mainly noted during daytime hours when effect of vegetation on air temperature through evapotranspiration and shadowing is major. The extra cooling simulated with Tree-PLEI is more marked at STOP 9, for which the tree coverage within the street canyon reaches 45%. Despite this general cooling trend, the simulated minimum temperatures remain overestimated even with Tree-PLEI (Fig. 9).

The temporal variations of wind speed (Figs. 9c,d), which is very low during the entire IOP, are hard to capture by the model whatever the configuration resulting in R correlation coefficients lower than 0.24 for both stop points and all simulations because the measured wind speeds are low and variations are somehow random. Besides variations, wind speed intensity is overestimated on average by Veg-TOPO and Veg-PLEI with biases around +0.70 m s^{-1} (Table 6). Both

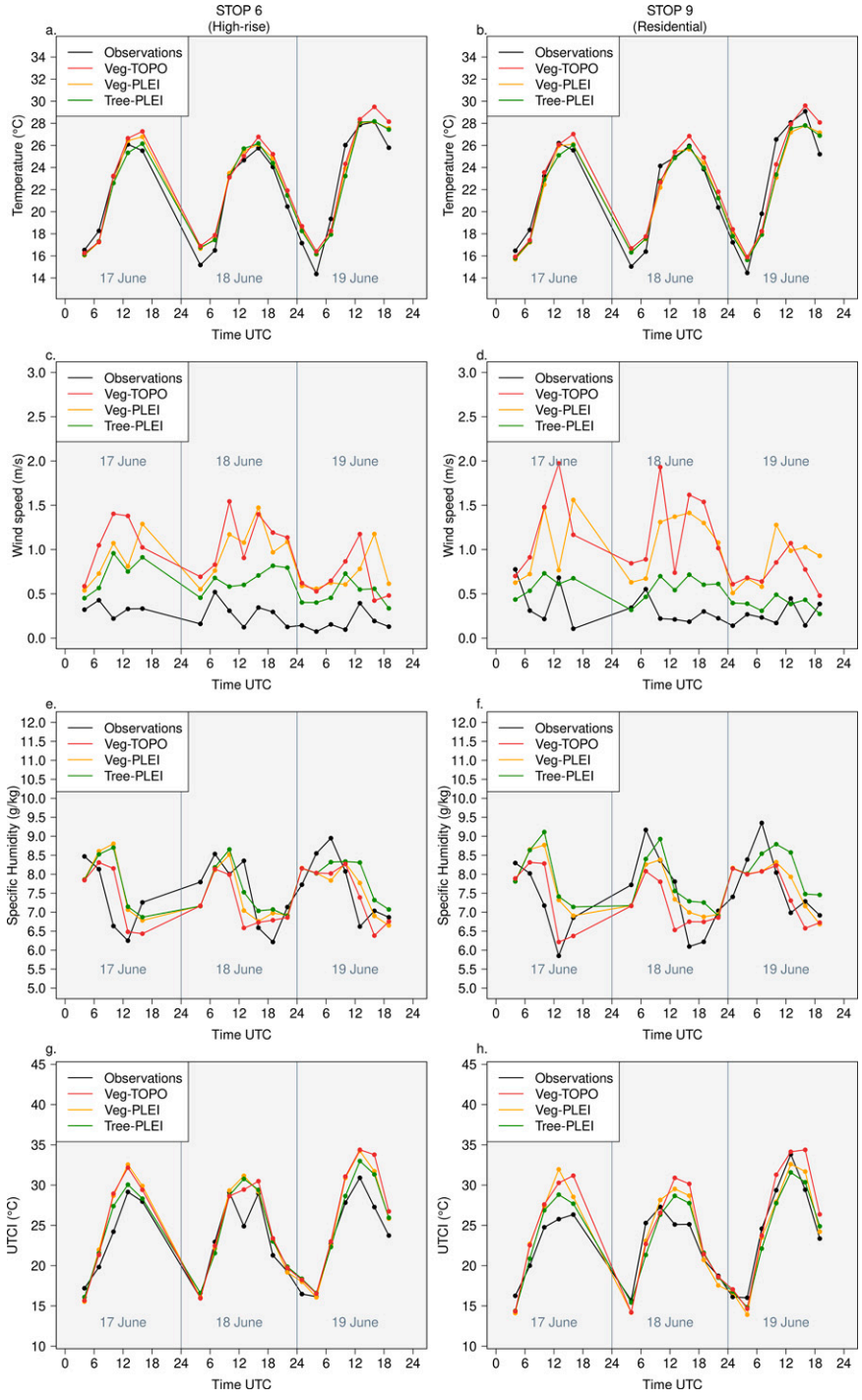

FIG. 9. Microclimatic variables at 2 m for (left) STOP 6 and (right) STOP 9: (a),(b) temperature; (c),(d) specific humidity; (e),(f) wind speed; and (g),(h) UTCI.

Veg-TOPO and Veg-PLEI simulate a wind speed diurnal cycle more marked than in observations with daily maximum between 1 and 2 m s^{-1}, whereas wind speed measurements are lower than 0.5 m s^{-1}. For STOP 9, Veg-TOPO and Veg-PLEI simulate higher maximum wind speed than for STOP 6 (1.7 vs 1.2 m s^{-1}, respectively), whereas measurements are comparable. This result may be explained by the highest building height of STOP 6, which already causes a slowing down of the airflow due to taller buildings. Tree-PLEI better performs at simulating wind speed at both stop points, with biases that are significantly smaller relative to Veg-TOPO and Veg-PLEI of 0.30 m s^{-1} for STOP 6 and 0.50 m s^{-1} for

TABLE 6. Comparison of scores (R, MBE, and RMSE) for STOP 6 and STOP 9 for the three simulation configurations: Veg-TOPO, Veg-PLEI, and Tree-PLEI.

	STOP 6			STOP 9		
	Veg-TOPO	Veg-PLEI	Tree-PLEI	Veg-TOPO	Veg-PLEI	Tree-PLEI
Temperature (°C)						
R^2	0.94	0.94	0.93	0.92	0.91	0.93
MBE	0.68	0.35	0.19	0.40	−0.19	−0.22
RMSE	1.30	1.11	1.16	1.34	1.35	1.23
Wind speed (m s^{-1})						
R^2	0.19	0.05	0.08	0.00	0.24	0.05
MBE	0.69	0.62	0.37	0.74	0.68	0.19
RMSE	0.76	0.68	0.41	0.87	0.82	0.32
Specific humidity (g kg^{-1})						
R^2	0.35	0.21	0.22	0.49	0.36	0.29
MBE	−0.14	0.06	0.21	−0.15	0.15	0.40
RMSE	0.72	0.81	0.80	0.69	0.77	0.90
UTCI (°C)						
R^2	0.91	0.91	0.90	0.87	0.86	0.86
MBE	1.87	1.70	1.25	1.49	0.70	0.14
RMSE	2.75	2.65	2.13	3.01	2.50	2.00

STOP 9. The diurnal magnitude in wind speed is much weaker due to the implementation of the drag effect of urban trees (Redon et al. 2020), which slows down the airflow within the canyon.

Figures 9e and 9f and Table 6 show that, whatever the configuration, TEB struggles to reproduce the daily cycle of the specific humidity, which is more complex than that of temperature. R Pearson coefficients are lower than 0.5 although the correlation seems marginally better at STOP 9 than at STOP 6. Nonetheless, Veg-TOPO and Veg-PLEI simulate specific humidities with orders of magnitude closer to those observed than Tree-PLEI with similar MBE and RMSE values of respectively −0.14 and 0.06 g kg^{-1} against an MBE of 0.30 g kg^{-1} and a RMSE of 0.85 g kg^{-1} on average for both stops for Tree-PLEI. These results show that the model correctly represents the order of magnitude of specific humidity at this scale. However, an improvement of the water transfers between vegetation, soil, and urban canopy, by integrating urban hydrology processes in the model could improve the dynamics of simulated specific humidity.

The thermal comfort is evaluated through the UTCI that is diagnosed in the model and derived from measurements (Figs. 9g,h). As for the previous micrometeorological variables, little difference is observed between STOP 6 and 9 for the measurement-based UTCI. In comparison, the UTCI simulated by Tree-PLEI is closer to observations than those simulated by Veg-TOPO and Veg-PLEI. This is observed in a more pronounced way at stop 9 (Fig. 9h), although it is applicable to both stops. For STOP 6, this leads to a more realistic UTCI simulated by Tree-PLEI, with a lower MBE (1.25°C) than for the Veg simulations (average MBE of 1.78°C) and RMSE of 2.13°C as compared with 2.65°C (Table 6). It is more pronounced at STOP 9 with a MBE of only 0.14°C and an error of 2.00°C for Tree-PLEI, Veg-TOPO and Veg-PLEI still overestimating UTCI with a MBE between 1.49° and 0.70°C and a RMSE of 2.50°C for Veg-PLEI and 3.01°C for Veg-TOPO.

The underestimation of UTCI at night by the TEB-Veg parameterization, whatever the database used (TOPO or PLEI), majorly visible between the 17 and 18 of June, is explained by both a significant presence of high vegetation in the environment of STOP 9 (34% of coverage; Table 5) and the uncompacted local morphology. As a result, this high vegetation intercepts and absorbs a large portion of incoming solar radiation during the day, with the consequence that it dissipates in the form of infrared radiation at night, which limits the decrease of UTCI unlike the air temperature. The lower wind speed still reinforces this effect. These effects are well taken into account by Tree-PLEI, hence its better performance on UTCI. Without taking into consideration tree foliage in TEB-Veg, less infrared radiation is emitted into the canyon, thus increasing the decrease in UTCI at night. For STOP 6 (Fig. 9g), this phenomenon is less visible due to urban morphology. Since buildings are higher, solar radiation is predominantly intercepted by buildings, so that less radiation is absorbed by vegetation in the urban canyon. In this case, infrared emissions by building facades are already important and well represented with Veg-TOPO and Veg-PLEI. Therefore, the improvement brought by TEB-Tree at STOP 6 is still noted but is less marked, despite a significant fraction of high vegetation (26%). In conclusion, this 3-day study highlights that TEB-Tree makes it possible to better simulate the role of high vegetation in local thermal condition through more realistic diurnal cycles of UTCI for different urban environments.

The evaluation of the sensitivity of model performances to the description of vegetation in such a heterogeneous urban area shows that the refinement of the surface database alone (with a more realistic spatial distribution of vegetation) does

not allow for all microclimatic variables to be improved. Only the air temperature is significantly better simulated during the day, whatever the morphology of the built environment. On the other hand, in addition to a refined surface database, the modeling of the different vegetation strata brings a second level of improvement: by simulating the radiative, energetic, and dynamical processes associated with the presence of trees in urban canyons, not only air temperature, but also wind speed and thermal comfort level are much better simulated.

3) THERMAL COMFORT VARIABILITY AT NEIGHBORHOOD SCALE

From these encouraging results and the good performances of Tree-PLEI at specific locations, the spatial variability of thermal comfort is investigated with this configuration. The aim is to compare thermal comfort conditions simulated with regard to the spatial variability of the neighborhood's land use. We concentrate on the part of the simulation area that is best documented (surface characteristics and micrometeorological observations) and for which more expertise is available throughout the evaluation area (orange area on Fig. 2). This area is highly heterogeneous in terms of urban morphology and vegetation coverage and strata. Figure 10 indeed illustrates that UTCI is highly correlated to urban morphology. Three zones with differences in UTCI can be distinguished in this area, both during the day and at night. Detached housing near the sports field mostly composed of grass and sparse trees (SPT) has the lowest UTCI. This open and ventilated area with high vegetation and low building density is mostly in the shade during daytime. At nighttime, UTCI is still the lowest at SPT. Since a park can have a cooling influence within a perimeter of 100–200 m (Zardo et al. 2017), advection of the air from this stadium with trees most likely induces lower UTCIs in SPT area. Residential and individual detached houses with gardens (HGD) have an intermediate UTCI relative to the whole neighborhood. Indeed, this open low-rise area is characterized by low building heights and fractions as well as high tree and grass fractions. Land-use characteristics are consistent with the simulated thermal comfort. Compact midrise buildings (MBD) and HBD are heavily built-up and paved areas with tall buildings. HBD can be more ventilated during the day while MBD is closer to road areas. While it would be expected to have more differences in comfort indices for these two areas, their proximity to road surfaces can increase the UTCI at daytime especially for MBD. Direct radiation for pedestrians in the street with no shading effect during daytime also has an important influence on thermal comfort in this area. This is why, MBD presents the highest UTCI at daytime. At night, majorly for HBD, the restitution of heat stored in these buildings with high wall surfaces increases the UTCI. Tendencies from daylight are very similar at night, with a 3°C amplitude for nighttime and daytime UTCIs.

This exercise showed that the simulated UTCI may vary greatly spatially, representing the high microclimate variability of a neighborhood. Besides, it demonstrates that thermal comfort of pedestrians is highly correlated to land use, and consequently rather higher in urbanized areas that lack

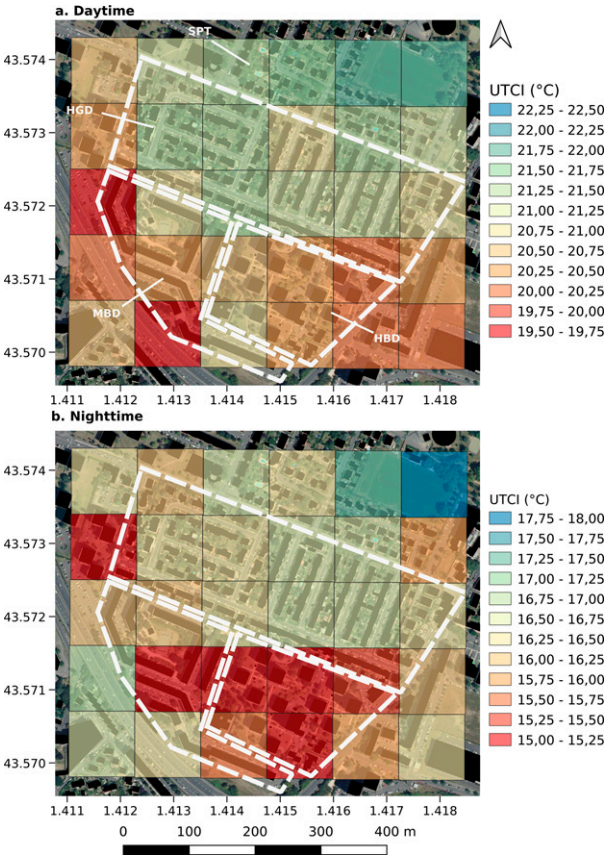

FIG. 10. Mean modeled UTCI over three hours and the three days of the IOP (17–19 Jun 2014) for Tree-PLEI for (a) daytime and (b) nighttime. Building surfaces are superimposed in black on these UTCI maps, and the white dotted line distinguishes the homogeneous neighborhoods of the evaluation area. The same color scale is used for two different ranges of temperatures, to highlight areas with similar thermal comfort tendencies.

vegetation. In regard to the Veg simulations, spatial and temporal variability decreases with the modeling of the tree strata (Tree-PLEI) results (not shown) but is more realistic and finer. At the scale of this small neighborhood of 600 m by 500 m, the comfort index is well represented. This configuration therefore allows a realistic level of thermal comfort to be achieved for preliminary urban landscape planning through simulation.

6. Conclusions

This study allowed us to quantify the effects both of a new parameterization of street trees implemented in TEB and a more detailed description of urban vegetation on the simulation of microclimatic variables and outdoor thermal comfort at the scale of a neighborhood consisting in different urban typologies. As far as developing a suitably detailed mapping of urban vegetation, this article presents a method applicable to any city with available data to create relevant land-use map for urban climate modeling use. It highlights that it is possible to build a well-documented urban vegetation database by treating

almost automatically easily accessible and high-resolution data from satellite imagery. The procedure consists in translating land cover into input parameters for TEB while considering associated assumptions. This methodology, applied to an urban neighborhood in the south of France, showed an overall accuracy of 63%, demonstrating its effectiveness.

Relying on the case study of a neighborhood of Toulouse, France, where in situ measurements were available, a sensitivity study was conducted to compare two vegetation parameterizations of the TEB model associated with vegetation databases with different accuracy. Improving the vegetation mapping and description while using the standard parameterization that does not treat vegetation as an additional stratum, provided more realistic but still overestimated simulated air temperatures. The detailed modeling of high vegetation and associated radiative, energetic, and dynamic physical processes gave even better results. In different parts of the neighborhood with significant density of high and low vegetation, simulation of air temperature with refined vegetation data and modeling was lower during the day and wind speed was reduced by drag effect of trees, in comparison with other simulations. Specific humidity was logically higher than that provided by the other simulation configurations but slightly overestimated relative to observations. The UTCI is particularly better simulated with the parameterization accounting for vegetation strata due to a better simulation of the variables from which it results, that is, temperature, wind, and mean radiant temperature. It is noted that, relative to previous less-refined simulation, it is able to reproduce the nocturnal and thermal comfort conditions in the different urban environments.

This study also highlighted the need to improve the humidity simulated by TEB, which could have a significant impact on the level of thermal comfort simulated. Nevertheless, specific humidity was not well represented either in the evaluation work of the synoptic meteorological conditions (appendix A). This variable is complex to model because it is related to the water cycle and depends on many variables. It could then raise a problem of the meteorological forcings at the limits of the domain or of the coupling model. It might require an improvement of the hydrological and thermal coupling in TEB, which is currently under way. This will also require special attention to be paid to soil texture databases, which will have an impact on microclimate modeling. They remain poorly informed in urban environment (Masson et al. 2020).

Our results suggest that our modeling configuration nevertheless reaches the limits of spatial resolution for which the model was designed. At this resolution and to further improve the calculation of the thermal comfort stress at finer-scale studies, TEB offers the possibility to couple microclimatic variables simulated to computational fluid dynamics models. Another point that could be stressed is the time of year (June) and the limited number of days for which the microclimatic observations were available: a longer dataset and encompassing warmer periods would allow a more robust evaluation of the ability of the model for reproducing thermal comfort in heterogeneous environment.

Last, as a result of its new parameterizations for differentiating vegetation strata, the urban canopy model TEB, if used with high-resolution and accurate databases describing the spatial distribution of vegetation and its different strata, has proven its ability to reproduce the urban climate even on a neighborhood scale. It is offering a powerful tool to better simulate urban microclimate and particularly thermal comfort in urban environments. Spatialized maps of thermal comfort for cities could then be provided to decision-makers in order to demonstrate quantitatively the interests of various greening strategies, thus allowing us to evaluate more realistically their impacts on thermal comfort.

Acknowledgments. We are grateful to Najla Touati (LISTT-CIEU of France) for providing us with a high-resolution cartography of urban vegetation derived from Pléiades satellite images, which served as a basis for this work. Also, the results presented in this publication have been made possible by observations collected during the research project EUREQUA (ANR-11-VILD-0006).

APPENDIX A

IGN BD TOPO Strata Selection

This appendix section highlights the choice of SIG layers used in the BD TOPO of the IGN for the study. This database is available freely online (https://geoservices.ign.fr/bdtopo). The data provided by BD TOPO are classified according to 10 characteristics: land use by road networks, railways and others, energy transmission network, hydrographical networks, buildings, vegetation, and administrative and activity areas, as well as topography and place names. For urban surface modeling purposes, we had to combine this information so as to distinguish land occupation by buildings, vegetation, asphalt, bare soil, and water surfaces (Table A1). For example, railways superimpose mostly natural bare soil, hence this category is associated with the land-use class bare soil. Energy transmission networks, orography, administrative, activity area, and place names layers are not used for this study because they do not provide land-cover information. The detail of each layer is associated with the format and the type of data in which it is provided by the IGN. For roads, paths and railways, the buffer associated with the linear information obtained is specified in column "Buffer."

APPENDIX B

Evaluation of Synoptic Meteorological Conditions

Synoptic conditions were evaluated in the first steps of the study (Fig. B1). It allowed us to evaluate the performance of the model to simulate the climatic conditions of the three days observed around the city, without the by urban influence. This comparison with observations from four meteorological stations around the city of Toulouse (see Fig. 5b for their locations in model 2) and model outputs demonstrates the capability of the MesoNH (Lafore et al. 1998) model to

TABLE A1. List of SIG layers from the BD TOPO of the IGN that were used to compile surface parameters for domain 3 (classified by their associated land use). The downloaded format and layer type are specified. A buffer is applied for linear layers on the basis of available information.

Name	Format	Type	Buffer	Land-use classification
BATI_INDIFFERENCIE	Shapefile	Surfacic	—	Buildings
BATI_INDUSTRIEL	Shapefile	Surfacic	—	
BATI_REMARQUABLE	Shapefile	Surfacic	—	
RESERVOIR	Shapefile	Surfacic	—	
CONSTRUCTION_LEGERE	Shapefile	Surfacic	—	
ROUTE	Shapefile	Linear	Width × 0.5	Asphalt
SURFACE_ROUTE	Shapefile	Surfacic	—	
POSTE_TRANSFORMATION	Shapefile	Surfacic	—	
CIMETIERE	Shapefile	Surfacic	—	
TRONCON_VOIE_FERREE	Shapefile	Linear	No.of ways × 2 m	Bare soil
CHEMIN	Shapefile	Linear	2 m (on each side)	
SURFACE_EAU	Shapefile	Surfacic	—	Water
ZONE_VEGETATION	Shapefile	Surfacic	—	Vegetation
TERRAIN_SPORT	Shapefile	Surfacic	—	

simulate atmospheric conditions and climatic variables for the days considered. The simulation configuration kept for this analysis is Veg-TOPO because the improvements made in the other simulations have no impact on the results outside model 3. Results are then not impacted by the choice of simulation configuration for urban vegetation.

Figure B1 air temperature is very well represented at synoptic stations. As expected, its diurnal evolution is coherent with observations (R^2 = 0.93) and errors are really low (with MBE of −0.21°C and RMSE of 1.29°C). Maximum daily temperatures are underestimated by a few degrees for day 1 and day 3, but minimum nocturnal temperatures are close to the one measured; 19 June was the hottest day. This warming trend at the end of IOP is also simulated by the model but underestimated. Modeled specific humidity ranges in the same amplitudes as the observations but does not represent a coherent daily cycle evolution. Meanwhile, wind speed is very close to station measurements with a RMSE of only 0.88 m s^{-1}. The model well simulates wind speed diurnal variations despite a very important standard deviation for the four stations. As a consequence, climatic parameters simulated on semirural areas are consistent with

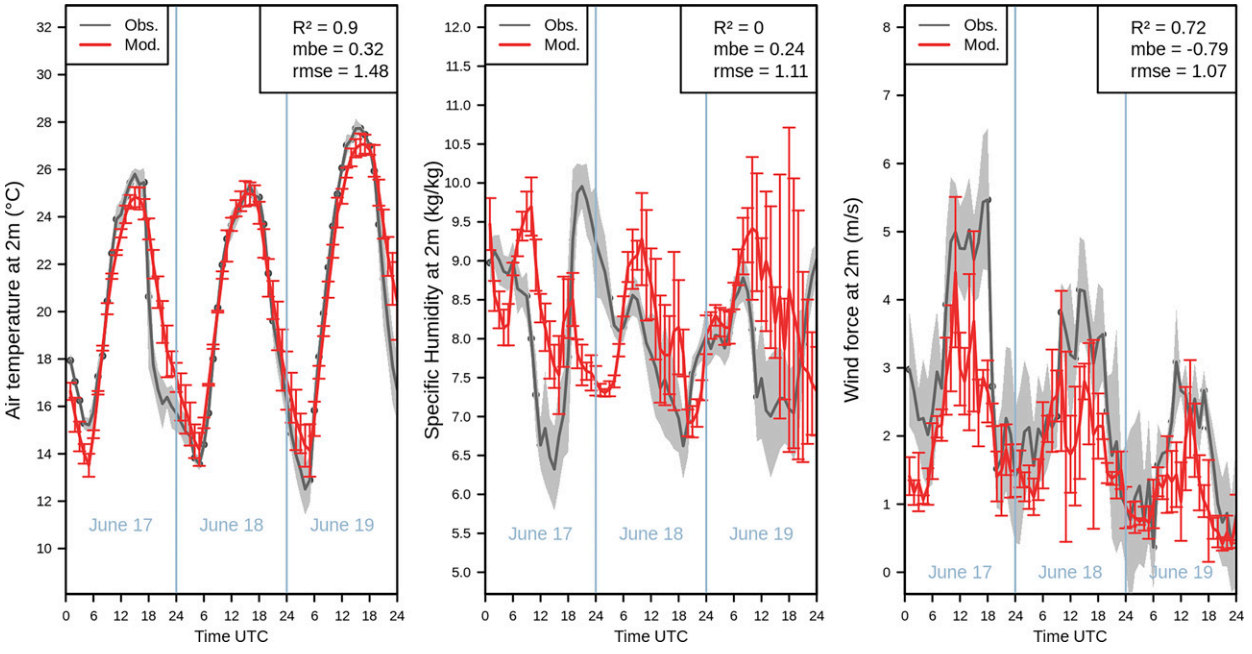

FIG. B1. Average microclimatic parameters for four synoptic stations, with their standard deviations, for (a) air temperature, (b) specific humidity, and (c) wind speed. Observations are in gray, and the standard model simulation configuration is in red.

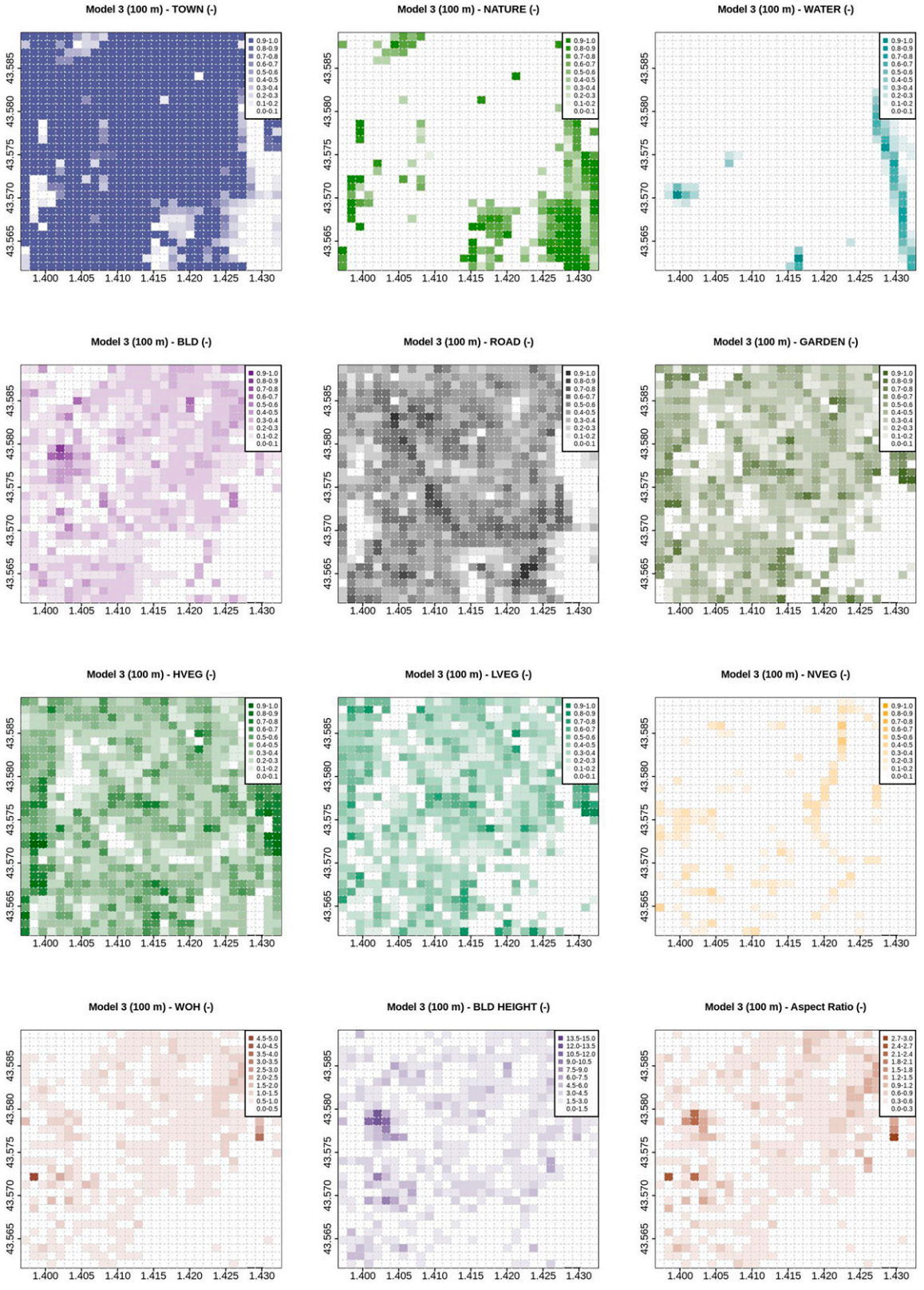

FIG. C1. Surface parameters for model 3.

TABLE D1. Comparison of scores (R, MBE, and RMSE) for STOP 1–STOP 5 and STOP 7–STOP 8 for the three simulation configurations: Veg-TOPO, Veg-PLEI, and Tree-PLEI.

	STOP 1			STOP 2			STOP 3			STOP 4			STOP 5			STOP 7			STOP 8		
	Veg-TOPO	Veg-PLEI	Tree-PLEI	Veg-TOPO	Veg-PLEI	Tree-PLEI	Veg-TOPO	Veg-PLEI	Tree-PLEI	Veg-TOPO	Veg-PLEI	Tree-PLEI	Veg-TOPO	Veg-PLEI	Tree-PLEI	Veg-TOPO	Veg-PLEI	Tree-PLEI	Veg-TOPO	Veg-PLEI	Tree-PLEI
Temperature (°C)																					
R	0.95	0.95	0.95	0.95	0.95	0.93	0.96	0.95	0.95	0.93	0.93	0.91	0.95	0.94	0.93	0.93	0.92	0.92	0.92	0.92	0.92
MBE	0.11	−0.52	−0.66	0.84	0.70	0.53	1.06	0.63	0.53	0.50	0.32	0.15	0.67	0.26	0.14	0.12	−0.39	−0.36	0.30	−0.15	−0.36
RMSE	1.15	1.41	1.50	1.34	1.25	1.31	1.40	1.15	1.10	1.35	1.28	1.37	1.25	1.17	1.26	1.34	1.49	1.49	1.31	1.30	1.35
Wind speed (m s^{-1})																					
R	0.38	0.49	0.69	0.03	0.00	0.04	0.03	0.08	0.02	0.12	0.03	0.11	0.02	0.20	0.15	0.16	0.14	0.00	0.01	0.03	0.08
MBE	0.56	0.33	0.11	0.81	0.81	0.57	0.68	0.53	0.26	0.68	0.70	0.31	0.92	0.92	0.42	0.81	0.80	0.49	0.91	0.77	0.32
RMSE	0.89	0.78	0.74	0.93	0.91	0.64	0.83	0.65	0.43	0.78	0.79	0.37	1.04	1.04	0.52	0.94	0.91	0.54	1.01	0.87	0.39
Specific humidity (g kg^{-1})																					
R	0.04	0.00	0.01	0.57	0.47	0.47	0.49	0.26	0.26	0.37	0.33	0.40	0.39	0.30	0.28	0.29	0.29	0.30	0.40	0.23	0.26
MBE	0.08	0.47	0.53	−0.12	0.03	0.12	−0.12	0.22	0.33	−0.11	0.11	0.16	−0.18	0.04	0.20	−0.46	−0.24	−0.11	−0.18	0.11	0.31
RMSE	0.72	0.97	1.02	0.51	0.54	0.54	0.56	0.71	0.76	0.64	0.66	0.63	0.66	0.67	0.70	0.87	0.74	0.71	0.75	0.86	0.88
UTCI (°C)																					
R	0.52	0.54	0.56	0.88	0.90	0.88	0.88	0.88	0.89	0.89	0.89	0.91	0.86	0.85	0.89	0.91	0.92	0.88	0.92	0.89	0.90
MBE	0.40	−0.04	−0.85	2.33	2.39	2.47	1.75	1.51	1.37	2.32	2.34	1.80	1.96	1.47	1.63	1.62	1.18	1.31	1.68	1.26	0.40
RMSE	5.83	5.72	5.73	3.73	3.74	3.77	3.03	2.87	2.55	3.22	3.28	2.42	3.39	3.02	2.65	2.93	2.37	2.69	3.12	2.96	1.79

observations at synoptic stations. After this step, the study focused on the modeling of urban effects with the TEB model, knowing that the modeling of specific humidity already presents a string bias at this scale.

APPENDIX C

Surface Parameters Provided as Input to Model 3

This appendix is designed to document the surface parameters defined for model 3 as they are defined as input parameters of the model. These maps of model 3 (Fig. C1) represent the fractions of each main type of surfaces in SURFEX: TOWN, NATURE, and WATER (no SEA in the study area). Then, there are urban characteristics with buildings, road, garden, high vegetation, low vegetation, and bare ground fractions. Morphological urban parameters such as wall density, building height, and building aspect ratio are also specified.

APPENDIX D

Evaluation Scores Comparison for the Other Seven Stop Points for Veg-TOPO, Veg-PLEI, and Tree-PLEI Simulations

This appendix aims at completing the scores of comparison of microclimate variables simulated on specific stop points as STOP 6 and STOP 9 are described in Table 6 of the main text. Table D1 compiles the scores of R, MBE, and RMSE for STOP 1–STOP 5 and STOP 7–STOP 8 for temperature, wind speed, specific humidity, and UTCI. Veg-TOPO and Veg-PLEI show slightly higher temperature variability agreement with observation than Tree-PLEI simulation for all stop points, but Tree-PLEI highlight better represented temperatures (lower MBE and RMSE). With the three configurations, the model encounters difficulties to reproduce variability and intensity of wind speed. However, intensity of wind speed is better represented with Tree-PLEI (MBE and RMSE lower for each stop points than those obtain with Veg-TOPO and Veg-PLEI simulations). Specific humidity results are not homogeneous; they depend on the stop points' land-use characteristics. None of the three simulations provide satisfactory results. The UTCI is better simulated with Tree-PLEI, which produces the best evaluation scores for most of the stop points.

REFERENCES

Armson, D., P. Stringer, and A. Ennos, 2012: The effect of tree shade and grass on surface and globe temperatures in an urban area. *Urban For. Urban Greening*, **11**, 245–255, https://doi.org/10.1016/j.ufug.2012.05.002.

Boone, A., J.-C. Calvet, and J. Noilhan, 1999: Inclusion of a third soil layer in a land surface scheme using the force–restore method. *J. Appl. Meteor.*, **38**, 1611–1630, https://doi.org/10.1175/1520-0450(1999)038<1611:IOATSL>2.0.CO;2.

Bossard, M., J. Feranec, and J. Otahel, 2000: CORINE land cover technical guide: Addendum 2000. EEA Tech. Rep. 40, 105 pp.

Bowler, D. E., L. Buyung-Ali, T. M. Knight, and A. S. Pullin, 2010: Urban greening to cool towns and cities: A systematic review of the empirical evidence. *Landscape Urban Plann.*, **97**, 147–155, https://doi.org/10.1016/j.landurbplan.2010.05.006.

Bröde, P., D. Fiala, K. Błażejczyk, I. Holmér, G. Jendritzky, B. Kampmann, B. Tinz, and G. Havenith, 2012: Deriving the operational procedure for the universal thermal climate index (UTCI). *Int. J. Biometeor.*, **56**, 481–494, https://doi.org/10.1007/s00484-011-0454-1.

Buttner, G., J. Feranec, G. Jaffrain, L. Mari, G. Maucha, and T. Soukup, 2004: The CORINE land cover 2000 project. *EARSeL eProc.*, **3**, 331–346.

Cleugh, H. A., and T. R. Oke, 1986: Suburban-rural energy balance comparisons in summer for Vancouver, B.C. *Bound.-Layer Meteor.*, **36**, 351–369, https://doi.org/10.1007/BF00118337.

Coutts, A. M., E. C. White, N. J. Tapper, J. Beringer, and S. J. Livesley, 2015: Temperature and human thermal comfort effects of street trees across three contrasting street canyon environments. *Theor. Appl. Climatol.*, **124**, 55–68, https://doi.org/10.1007/s00704-015-1409-y.

Crombette, P., 2016: Contribution des technologies satellitaires Pléiades à l'étude des trames vertes urbaines: Entre maintien des connectivités écologiques potentielles et densification des espaces urbains (Contribution of Pléiades satellite technologies to the study of urban greenways: Between maintaining potential ecological connectivity and densification of urban spaces). Ph.D. thesis, Université Toulouse–Jean Jaurès, 344 pp., https://tel.archives-ouvertes.fr/tel-01503506v2/document.

——, S. Le Corre, and C. Tinel, 2014: Traitement d'images satellitaires à très haute résolution spatiale et identification de zones à enjeux dans l'aménagement des trames vertes urbaines (Processing satellite images with very high spatial resolution and identification of conflict areas in the management of urban green networks). *Rev. Fr. Photogramm. Télédétect.*, **208**, 19–25, https://doi.org/10.52638/rfpt.2014.130.

Decharme, B., A. Boone, C. Delire, and J. Noilhan, 2011: Local evaluation of the interaction between soil biosphere atmosphere soil multilayer diffusion scheme using four pedotransfer functions. *J. Geophys. Res.*, **116**, D20126, https://doi.org/10.1029/2011JD016002.

de Munck, C., A. Lemonsu, V. Masson, J. L. Bras, and M. Bonhomme, 2018: Evaluating the impacts of greening scenarios on thermal comfort and energy and water consumptions for adapting Paris city to climate change. *Urban Climate*, **23**, 260–286, https://doi.org/10.1016/j.uclim.2017.01.003.

Faroux, S., A. Kaptué Tchuenté, J.-L. Roujean, V. Masson, E. Martin, and P. L. Moigne, 2013: ECOCLIMAP-II/Europe: A twofold database of ecosystems and surface parameters at 1 km resolution based on satellite information for use in land surface, meteorological and climate models. *Geosci. Model Dev.*, **6**, 563–582, https://doi.org/10.5194/gmd-6-563-2013.

Grimmond, C. S. B., and Coauthors, 2010: The International Urban Energy Balance Models Comparison Project: First results from phase 1. *J. Appl. Meteor. Climatol.*, **49**, 1268–1292, https://doi.org/10.1175/2010JAMC2354.1.

——, and Coauthors, 2011: Initial results from phase 2 of the International Urban Energy Balance Model Comparison. *Int. J. Climatol.*, **31**, 244–272, https://doi.org/10.1002/joc.2227.

Grimmond, S., 2007: Urbanization and global environmental change: Local effects of urban warming. *Geogr. J.*, **173**, 83–88, https://doi.org/10.1111/j.1475-4959.2007.232_3.x.

Hamdi, R., and V. Masson, 2008: Inclusion of a drag approach in the Town Energy Balance (TEB) scheme: Offline 1D evaluation in a street canyon. *J. Appl. Meteor. Climatol.*, **47**, 2627–2644, https://doi.org/10.1175/2008JAMC1865.1.

Haouès-Jouve, S., and Coauthors, 2022: Cross-analysis for the assessment of urban environmental quality: An interdisciplinary and participative approach. *Environ. Plann.*, **49B**, 1024–1047, https://doi.org/10.1177/23998083211037350.

Joshi, D. N., and A. Joshi, 2015: Role of urban trees in amelioration of temperatures. *Int. J. Res. Stud. Biosci.*, **3**, 132–137.

Krayenhoff, E., A. Christen, A. Martilli, and T. Oke, 2014: A multi-layer radiation model for urban neighbourhoods with trees. *Bound.-Layer Meteor.*, **151**, 139–178, https://doi.org/10.1007/s10546-013-9883-1.

Krayenhoff, E. S., J.-L. Santiago, A. Martilli, A. Christen, and T. R. Oke, 2015: Parametrization of drag and turbulence for urban neighbourhoods with trees. *Bound.-Layer Meteor.*, **156**, 157–189, https://doi.org/10.1007/s10546-015-0028-6.

——, and Coauthors, 2020: A multi-layer urban canopy meteorological model with trees (BEP-tree): Street tree impacts on pedestrian-level climate. *Urban Climate*, **32**, 100590, https://doi.org/10.1016/j.uclim.2020.100590.

Kwok, Y. T., R. Schoetter, K. K.-L. Lau, J. Hidalgo, C. Ren, G. Pigeon, and V. Masson, 2019: How well does the local climate zone scheme discern the thermal environment of Toulouse (France)? An analysis using numerical simulation data. *Int. J. Climatol.*, **39**, 5292–5315, https://doi.org/10.1002/joc.6140.

Lafore, J.-P., and Coauthors, 1998: The Meso-NH Atmospheric Simulation System. Part I: Adiabatic formulation and control simulations. *Ann. Geophys.*, **16**, 90–109, https://doi.org/10.1007/s00585-997-0090-6.

Landis, J. R., and G. G. Koch, 1977: The measurement of observer agreement for categorical data. *Biometrics*, **33**, 159, https://doi.org/10.2307/2529310.

Le Bras, J., 2015: Le micro-climat urbain à haute résolution: Mesures et modélisation (The high-resolution urban microclimate: Measurements and modeling). Ph.D. thesis, Université de Toulouse, 208 pp., http://thesesups.ups-tlse.fr/2759/1/2015TOU30078.pdf.

Lee, S.-H., and S.-U. Park, 2008: A vegetated urban canopy model for meteorological and environmental modelling. *Bound.-Layer Meteor.*, **126**, 73–102, https://doi.org/10.1007/s10546-007-9221-6.

——, and J.-J. Baik, 2011: Evaluation of the Vegetated Urban Canopy Model (VUCM) and its impacts on urban boundary layer simulation. *Asia-Pac. J. Atmos. Sci.*, **47**, 151–165, https://doi.org/10.1007/s13143-011-0005-z.

——, H. Lee, S.-B. Park, J.-W. Woo, D.-I. Lee, and J.-J. Baik, 2016: Impacts of in-canyon vegetation and canyon aspect ratio on the thermal environment of street canyons: Numerical investigation using a coupled WRF-VUCM model. *Quart. J. Roy. Meteor. Soc.*, **142**, 2562–2578, https://doi.org/10.1002/qj.2847.

Lemonsu, A., C. S. B. Grimmond, and V. Masson, 2004: Modeling the surface energy balance of the core of an old Mediterranean city: Marseille. *J. Appl. Meteor.*, **43**, 312–327, https://doi.org/10.1175/1520-0450(2004)043<0312:MTSEBO>2.0.CO;2.

——, V. Masson, L. Shashua-Bar, E. Erell, and D. Pearlmutter, 2012: Inclusion of vegetation in the Town Energy Balance model for modelling urban green areas. *Geosci. Model Dev.*, **5**, 1377–1393, https://doi.org/10.5194/gmd-5-1377-2012.

——, and Coauthors, 2019: Comparison of microclimate measurements and perceptions as part of a global evaluation of environmental quality at neighbourhood scale. *Int. J. Biometeor.*, **64**, 265–276, https://doi.org/10.1007/s00484-019-01686-1.

Masson, V., 2000: A physically-based scheme for the urban energy budget in atmospheric models. *Bound.-Layer Meteor.*, **94**, 357–397, https://doi.org/10.1023/A:1002463829265.

——, and Y. Seity, 2009: Including atmospheric layers in vegetation and urban offline surface schemes. *J. Appl. Meteor. Climatol.*, **48**, 1377–1397, https://doi.org/10.1175/2009JAMC1866.1.

——, and Coauthors, 2013: The SURFEXv7.2 land and ocean surface platform for coupled or offline simulation of Earth surface variables and fluxes. *Geosci. Model Dev.*, **6**, 929–960, https://doi.org/10.5194/gmd-6-929-2013.

——, and Coauthors, 2020: City-descriptive input data for urban climate models: Model requirements, data sources and challenges. *Urban Climate*, **31**, 100536, https://doi.org/10.1016/j.uclim.2019.100536.

Meili, N., and Coauthors, 2020: An urban ecohydrological model to quantify the effect of vegetation on urban climate and hydrology (UT&C v1.0). *Geosci. Model Dev.*, **13**, 335–362, https://doi.org/10.5194/gmd-13-335-2020.

——, and Coauthors, 2021: Tree effects on urban microclimate: Diurnal, seasonal, and climatic temperature differences explained by separating radiation, evapotranspiration, and roughness effects. *Urban For. Urban Greening*, **58**, 126970, https://doi.org/10.1016/j.ufug.2020.126970.

Mills, G., 2008: Luke Howard and *The Climate of London*. *Weather*, **63**, 153–157, https://doi.org/10.1002/wea.195.

Mussetti, G., and Coauthors, 2020: COSMO-BEP-Tree v1.0: A coupled urban climate model with explicit representation of street trees. *Geosci. Model Dev.*, **13**, 1685–1710, https://doi.org/10.5194/gmd-13-1685-2020.

Oke, T., 1988: The urban energy balance. *Prog. Phys. Geogr.*, **12**, 471–508, https://doi.org/10.1177/030913338801200401.

Qiu, G. Y., H. Li, Q. Zhang, W. Chen, X. Liang, and X. Li, 2013: Effects of evapotranspiration on mitigation of urban temperature by vegetation and urban agriculture. *J. Integr. Agric.*, **12**, 1307–1315, https://doi.org/10.1016/S2095-3119(13)60543-2.

Redon, E. C., A. Lemonsu, V. Masson, B. Morille, and M. Musy, 2017: Implementation of street trees within the solar radiative exchange parameterization of TEB in SURFEX v8.0. *Geosci. Model Dev.*, **10**, 385–411, https://doi.org/10.5194/gmd-10-385-2017.

Redon, E., A. Lemonsu, and V. Masson, 2020: An urban trees parameterization for modeling microclimatic variables and thermal comfort conditions at street level with the Town Energy Balance model (TEB-SURFEX v8.0). *Geosci. Model Dev.*, **13**, 385–399, https://doi.org/10.5194/gmd-13-385-2020.

Ryu, Y.-H., E. Bou-Zeid, Z.-H. Wang, and J. Smith, 2015: Realistic representation of trees in an urban canopy model. *Bound.-Layer Meteor.*, **159**, 193–220, https://doi.org/10.1007/s10546-015-0120-y.

Shashua-Bar, L., and M. Hoffman, 2000: Vegetation as a climatic component in the design of an urban street. *Energy Build.*, **31**, 221–235, https://doi.org/10.1016/S0378-7788(99)00018-3.

——, I. X. Tsiros, and M. E. Hoffman, 2010: A modeling study for evaluating passive cooling scenarios in urban streets with trees. Case study: Athens, Greece. *Build. Environ.*, **45**, 2798–2807, https://doi.org/10.1016/j.buildenv.2010.06.008.

Upmanis, H., I. Eliasson, and S. Lindqvist, 1998: The influence of green areas on nocturnal temperatures in a high latitude city (Göteborg, Sweden). *Int. J. Climatol.*, **18**, 681–700, https://doi.org/10.1002/(SICI)1097-0088(199805)18:6<681::AID-JOC289>3.0.CO;2-L.

Wang, C., Z.-H. Wang, and J. Yang, 2018: Cooling effect of urban trees on the built environment of contiguous United States. *Earth's Future*, **6**, 1066–1081, https://doi.org/10.1029/2018EF000891.

——, ——, and Y.-H. Ryu, 2021: A single-layer urban canopy model with transmissive radiation exchange between trees and street canyons. *Build. Environ.*, **191**, 107593, https://doi.org/10.1016/j.buildenv.2021.107593.

Wang, Z.-H., E. Bou-Zeid, and J. A. Smith, 2012: A coupled energy transport and hydrological model for urban canopies evaluated using a wireless sensor network. *Quart. J. Roy. Meteor. Soc.*, **139**, 1643–1657, https://doi.org/10.1002/qj.2032.

Yamada, T., 1982: A numerical model study of turbulent airflow in and above a forest canopy. *J. Meteor. Soc. Japan*, **60**, 439–454, https://doi.org/10.2151/jmsj1965.60.1_439.

Zardo, L., D. Geneletti, M. Pérez-Soba, and M. V. Eupen, 2017: Estimating the cooling capacity of green infrastructures to support urban planning. *Ecosyst. Serv.*, **26**, 225–235, https://doi.org/10.1016/j.ecoser.2017.06.016.